Crucial Role of the SH2B1 PH Domain for the Control of Energy Balance

Anabel Flores,[1] Lawrence S. Argetsinger,[2] Lukas K.J. Stadler,[3] Alvaro E. Malaga,[2] Paul B. Vander,[2] Lauren C. DeSantis,[2] Ray M. Joe,[1,2] Joel M. Cline,[2] Julia M. Keogh,[3] Elana Henning,[3] Ines Barroso,[4] Edson Mendes de Oliveira,[3] Gowri Chandrashekar,[2] Erik S. Clutter,[2] Yixin Hu,[2] Jeanne Stuckey,[5] I. Sadaf Farooqi,[3] Martin G. Myers Jr.,[1,2,6] and Christin Carter-Su[1,2,6]

Disruption of the adaptor protein SH2B1 (SH2-B, PSM) is associated with severe obesity, insulin resistance, and neurobehavioral abnormalities in mice and humans. Here, we identify 15 *SH2B1* variants in severely obese children. Four obesity-associated human *SH2B1* variants lie in the Pleckstrin homology (PH) domain, suggesting that the PH domain is essential for SH2B1's function. We generated a mouse model of a human variant in this domain (P322S). P322S/P322S mice exhibited substantial prenatal lethality. Examination of the P322S/+ metabolic phenotype revealed late-onset glucose intolerance. To circumvent P322S/P322S lethality, mice containing a two-amino acid deletion within the SH2B1 PH domain (ΔP317, R318 [ΔPR]) were studied. Mice homozygous for ΔPR were born at the expected Mendelian ratio and exhibited obesity plus insulin resistance and glucose intolerance beyond that attributable to their increased adiposity. These studies demonstrate that the PH domain plays a crucial role in how SH2B1 controls energy balance and glucose homeostasis.

Hyperphagia, severe obesity, insulin resistance, and neurobehavioral abnormalities have been reported in individuals with rare coding variants in the gene encoding SH2B1 (SH2-B, PSM) (1,2). Consistently, mice null for *Sh2b1* exhibit obesity, impaired glucose homeostasis, and often, aggressive behavior (3–5). Transgenic expression of the β-isoform of SH2B1 (SH2B1β) in the brain largely corrects the obesity and glucose intolerance of otherwise *Sh2b1*-null mice (6), suggesting the importance of brain SH2B1 for the control of energy balance and glucose homeostasis.

At the cellular level, SH2B1 is an intracellular adaptor protein that is recruited to phosphorylated tyrosine residues on specific membrane receptor tyrosine kinases (e.g., receptors for brain-derived neurotrophic factor [BDNF], nerve growth factor [NGF], insulin) and cytokine receptor/Janus kinase (JAK) complexes (e.g., leptin receptor/JAK2) and enhances the function of these receptors (7–13). The exact mechanism(s) by which it does so is unclear, although a variety of mechanisms have been proposed. These include enhanced dimerization causing increased activation of the kinase itself (14), stabilization of the active state of the kinase (15), decreased dephosphorylation or increased complex formation of insulin receptor substrate (IRS) proteins bound to receptors or receptor/JAK2 (16,17), regulation of the actin cytoskeleton (18), and activation of specific pathways, including extracellular signal–regulated kinases (ERKs), Akt, and/or phospholipase Cγ (10,19). Some of these receptors, including the leptin, BDNF, and insulin receptors, play important roles in the central control of energy expenditure and/or glucose homeostasis (20). SH2B1β has been shown to enhance BDNF- and NGF-stimulated neurite outgrowth in PC12 cells (13,21).

The four isoforms of SH2B1 (α, β, γ, δ), which differ only in their COOH termini, share 631 NH₂-terminal

amino acids. These amino acids possess a dimerization domain, Pleckstrin homology (PH) domain, src-homology 2 (SH2) domain, nuclear localization sequence (NLS), and nuclear export sequence (NES) (22–24) (Fig. 1A). The SH2 domain enables SH2B1 recruitment to specific phosphorylated tyrosine residues in activated tyrosine kinases (25). The NLS and NES are essential for SH2B1 to shuttle among the nucleus, the cytosol, and the plasma membrane (22,23). The NLS combined with the dimerization domain enables SH2B1 to associate with the plasma membrane (26). However, the function and importance of the SH2B1 PH domain remains largely unknown. Four human obesity-associated variants lie in the SH2B1 PH domain (Fig. 1A), suggesting the importance of the PH domain in SH2B1 function. The PH domains of some proteins bind inositol phospholipids to mediate membrane localization (27,28). However, 90–95% of all human PH domains do not bind strongly to phosphoinositides and presumably mediate other functions (29). Indeed, the PH domain of SH2B1 neither localizes to the plasma membrane nor is required to localize SH2B1β to the plasma membrane (23,30). Here, we tested the importance of the PH domain of SH2B1 in vivo by generating and studying mice containing human obesity-associated (P322S) or engineered (in-frame deletion of P317 and R318 [ΔPR]) mutations in the SH2B1 PH domain. Our results demonstrate that the SH2B1 PH domain plays multiple crucial roles in vivo, including for the control of energy balance and glucose homeostasis, and in in vitro studies, changes the subcellular distribution of SH2B1β and enhances NGF-stimulated neurite outgrowth in PC12 cells.

RESEARCH DESIGN AND METHODS

Human Studies
The Genetics of Obesity Study (GOOS) is a cohort of >7,000 individuals with severe obesity with age of onset of <10 years (31,32). Severe obesity is defined as a BMI (kg/m^2) SD score >3 (U.K. reference population). Whole-exome sequencing and targeted resequencing were performed as in Hendricks et al. (33). All variants were confirmed by Sanger sequencing (1). HOMA of insulin resistance (HOMA-IR) was calculated using the equation HOMA-IR score = [(fasting insulin in μU/mL) × (fasting glucose in mg/dL)] / 405, which estimates steady-state β-cell function and insulin sensitivity (34,35). All human studies were approved by the Cambridge local research ethics committee. Each subject (or parent for those <16 years of age) provided written informed consent; minors provided oral consent.

Animal Care
Animal procedures were approved by the University of Michigan Committee on the Use and Care of Animals in accordance with Association for Assessment and Accreditation of Laboratory Animal Care and National Institutes of Health guidelines. Mice were bred at the University of Michigan and housed in ventilated cages at 23°C on a 12-h light (0600–1800 h)/12-h dark cycle with ad libitum

access to food and tap water except as noted. Mice were fed standard chow (20% protein, 9% fat [PicoLab Mouse Diet 20 5058, #0007689]) or, as described in Fig. 2H–M and Supplementary Fig. 2F–K, a high-fat diet (HFD) (20% protein, 20% carbohydrate, 60% fat [D12492; Research Diets]).

Mouse Models, Genotyping, and Gene Expression
CRISPR/Cas9 genome editing was used to insert the P322S mutation into mice. The reverse complement of the genomic Sh2b1 sequence in C57BL/6J mice (accession number NC_000073, GRC m38) was used to design the reagents for CRISPR. The guides were designed using the website described in Ran et al. (36). The mutations in the donor are summarized in Fig. 1C (details in the Supplementary Data). After testing, each guide/donor combination was injected into C57BL/6J oocytes by the University of Michigan Transgenic Animal Model Core. P322S and ΔPR founders were backcrossed to C57BL/6J mice. The mice were genotyped as described in Truett et al. (37) using primers listed in Supplementary Table 1. The P322S and ΔPR PCR products were digested with XbaI or purified and sequenced. Sh2b1 knockout (KO) mice were obtained from Dr. Liangyou Rui (University of Michigan) and genotyped according to Duan et al. (3). C57BL/6J mice used to invigorate our C57BL/6J colony came from The Jackson Laboratory. Relative levels of Sh2b1 gene expression were determined using RT-PCR (details in the Supplementary Data).

Mouse Body Weight and Food Intake
Mice were individually housed, and body weight and food consumption were assessed weekly.

Mouse Glucose Tolerance Tests, Insulin Tolerance Tests, and Hormone Levels
Mice were fasted 0900–1300 h for glucose tolerance tests (GTTs) or 0800–1400 h for insulin tolerance tests (ITTs). Glucose or human insulin was injected intraperitoneally, and blood was collected from the tail vein. Blood glucose levels were assessed using a Bayer Contour glucometer. For plasma insulin levels, mice were fasted 0800–1400 h, and tail blood was assayed using an Ultra Sensitive Mouse Insulin ELISA kit (#90080; Crystal Chem). Tail blood (0900–1000 h) (Figs. 2F and 4G) or trunk blood after sacrifice (1000–1300 h) (Fig. 6B) from fed mice was tested for leptin using a Mouse Leptin ELISA kit (#90030; Crystal Chem).

Mouse Body Composition, Metabolic Assessment, and Tissue Collection
Body composition was measured at room temperature in the morning or evening (Fig. 6A) using a Minispec LF90 II Bruker Optics nuclear magnetic resonance (NMR) analyzer (University of Michigan Animal Phenotyping Core). To assess metabolic state, mice were single-housed for 3 days and then tested for 72 h using a Comprehensive Lab Animal Monitoring System (Columbus Instruments). O$_2$ consumption (VO$_2$), CO$_2$ production (VCO$_2$), X activity, and Z activity were collected in 20-min bins. The final 24 h of recordings are presented. Mice were sacrificed
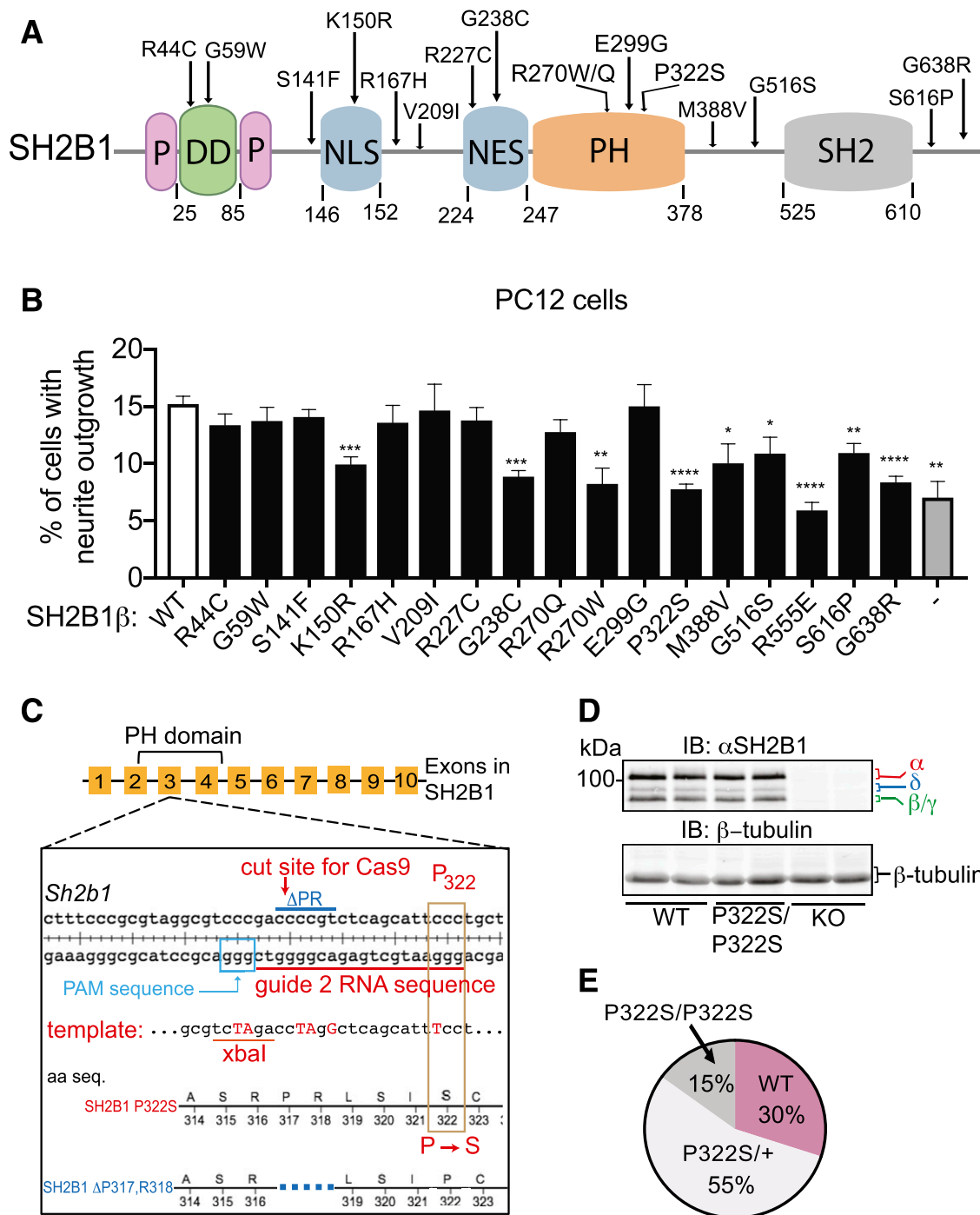
Figure 1—Identification of *SH2B1* variants and generation of P322S mice. *A*: Human SH2B1 protein (NP_001139268). Amino acid residues for newly characterized human obesity-associated SH2B1 variants and the previously characterized variant P322S are shown. DD, dimerization domain; P, proline-rich region. *B*: SH2B1 mutations impair the ability of SH2B1 to enhance neurite outgrowth. PC12 cells transiently coexpressing GFP and either empty pcDNA3.1(+) vector (−), human SH2B1β WT, or SH2B1β mutant were treated with 20 ng/mL rat NGF for 3 days, after which neurite outgrowth was assessed. R555E lacking an intact SH2 domain and the human mutation P322S reported previously were included as positive controls. GFP-positive cells were scored for the presence of neurites two times the length of the cell body (≥400 cells/condition/experiment). The percentage of cells with neurites was determined by dividing the number of GFP-positive cells with neurites by the total number of GFP-positive cells. Data are mean ± SEM ($n = 5$). Each construct was compared with WT using a two-tailed Student t test. $*P < 0.05$, $**P < 0.01$, $***P < 0.001$, $****P < 0.0001$. *C*: CRISPR/Cas9 schematic for *Sh2b1* P322S gene editing. RNA guide sequence, PAM sequence, and cut site for Cas9 are shown for guide 2. The region of the 180-nucleotide oligo donor template used to direct homology-directed repair in the vicinity of the ΔPR deletion and P322 is shown. Mutations in donor template that introduce the C>T mutation to code for P322S and silent mutations to create a diagnostic XbaI site and disrupt guide RNA binding following repair are highlighted in red. aa seq., amino acid sequence. *D*: Proteins in brain tissue lysates from *Sh2b1* WT, P322S/P322S, and KO male mice were immunoblotted with αSH2B1 or αβ-tubulin. Migration of the 100-kDa protein standard and the four isoforms of SH2B1 are shown. IB, immunoblot. *E*: P322S/P322S mice from intercrosses of heterozygous mice were born at approximately one-half of the expected Mendelian ratio. $P < 0.05$, χ^2 test. $n = 179$ mice.

(1000–1300 h) using decapitation under isoflurane. Trunk blood was collected and the serum stored at −80°C. Tissues were collected, weighed, cryopreserved in liquid nitrogen, and stored at −80°C.

Immunoblotting

Frozen tissues were lysed in L-RIPA lysis buffer (50 mM Tris, 150 mM NaCl, 2 mM EGTA, 0.1% Triton X-100, pH 7.2 containing 1 mM Na_3VO_4, 1 mM PMSF, 10 μg/mL aprotinin, 1 μg/mL leupeptin). Equal amounts of protein were immunoblotted with antibody to SH2B1 (αSH2B1) (sc-136065, RRID:AB_2301871; Santa Cruz Biotechnology) (1:1,000 dilution) or β-tubulin (sc-55529, RRID:AB_2210962; Santa Cruz Biotechnology) (1:1,000 dilution) as described in Joe et al. (19). For immunoprecipitations, tissue lysates containing equal amounts of protein were incubated with αSH2B1 (1:100) and immunoprecipitated and immunoblotted as in Joe et al. PC12 cells (ATCC) were cultured and treated as in Joe et al. Briefly, the cells were grown in PC12 medium A (RPMI medium, 5% FBS, 10% heparan sulfate) in 10-cm dishes coated with rat tail type I collagen (#354236; Corning). Cells were transfected and, 24 h later, incubated overnight in deprivation medium (RPMI medium, 2% heparan sulfate, 1% FBS) before being lysed and immunoblotted with αSH2B1.

Live Cell Imaging

The indicated construct was transiently transfected into 293T cells or PC12 cells. Cells were treated and live cell images captured by confocal microscopy using an Olympus FV500 laser scanning microscope and FluoView version 5.0 software, as in Joe et al. (19).

Neurite Outgrowth

For Fig. 3D, PC12 cells were plated in six-well collagen-coated dishes, transiently transfected as indicated for 24 h, and incubated overnight in deprivation medium. Cells were treated, and neurite outgrowth was determined as in Joe et al. (19). For Fig. 1B, PC12 cells were treated as in Joe et al., with modifications described in the Supplementary Data.

Structural Modeling and ClustalW Analysis

A structural model for human SH2B1 was created by overlaying the PH domain sequence of human SH2B1 onto the mouse NMR structure of APS (Protein Data Bank ID 1V5M) using the PyMOL Molecular Graphics System version 2.2.3. ClustalW alignments were performed using LaserGene version 14.0.0 (DNASTAR, Madison, WI). Functional homology was defined as residues that match the consensus within 1 distance unit using the PAM250 mutation probability matrix.

Statistics

All nonhuman analyses were carried out using GraphPad Prism software. Body weight, GTTs, and ITTs were analyzed by two-way ANOVA followed by Fisher least significant difference posttest. Food intake was analyzed by linear regression. Significance of the deviation of birth rate from the expected Mendelian ratio was assessed using χ^2 test. For other physiological parameters, experimental animals were compared with their wild-type (WT) littermates by two-tailed Student t test. Neurite outgrowth was analyzed by a two-tailed Student t test. For all comparisons, $P < 0.05$ was considered significant.

Data and Resource Availability

Any raw data sets generated during the current study are available from the corresponding author on reasonable request, with all reagent and analytical details included in the published article (and its Supplementary Data). The mouse models generated and analyzed during the current study are available from the corresponding author upon reasonable request.

RESULTS

Identification and Characterization of 15 Rare Human Variants in *SH2B1*

Using exome sequencing, targeted resequencing, and Sanger sequencing of 3,000 individuals exhibiting severe obesity before the age of 10 years (33), we identified 15 rare variants in *SH2B1* in 16 unrelated individuals (Table 1 and Fig. 1A). Eleven variants are newly identified, while four (R227C, R270W, E299G, V209I) have been previously reported in other obese individuals but not well characterized (4,38,39). Fourteen of these variants are in the first 631 amino acids shared by all isoforms of SH2B1. The mean ± SD BMI SD score of variant carriers was 4.0 ± 0.6. The 15th variant causes the G638R mutation in the COOH-terminal tail unique to the β-isoform of SH2B1. A number of the *SH2B1* variant carriers had HOMA-IR (34,35) scores of >1.9, indicating insulin resistance and increased risk of type 2 diabetes (40). Some of the HOMA-IR scores, including those for people carrying three variants in or near the PH domain (G238C, R270Q, and M388V), were particularly high. A spectrum of neurobehavioral abnormalities, including learning difficulties, dyspraxia, hyperactivity/inattention, aggression/emotional lability, anxiety, and autistic traits, were detected in all the individuals for whom behavioral information was available (Table 1). In the neurite outgrowth assay, 7 of these 15 rare variants impaired the ability of SH2B1β to stimulate NGF-induced neurite outgrowth (Fig. 1B), suggesting that many of the variants negatively affect the neuronal function of SH2B1. Because the variants are found in multiple domains in SH2B1 and throughout the SH2B1 sequence, it is not surprising that individuals with different SH2B1 variants have different phenotypes. These newly characterized variants add support to SH2B1 being an important regulator of human body weight, insulin sensitivity, and behavior. Interestingly, four of the human obesity-associated *SH2B1* variants lie in the PH domain of SH2B1, suggesting the importance of the PH domain in the ability of SH2B1 to regulate energy balance, glucose metabolism, and behavior.

Table 1—Phenotypes seen in carriers of rare variants in *SH2B1*

SH2B1 variant	MAF (%)	Age (years)	Sex	BMI (SD)	Leptin (ng/mL)	HOMA-IR	Learning difficulties, speech and language delay	Dyspraxia	Hyperactivity/ inattention	Aggression/ emotional lability	Anxiety	Autistic traits
R44C (c.130C>T)	0.005	4.7	F	29 (4.7)	25.1	2.7	+ S	+	+	+	+	+
G59W (c.175 G>T)	0*	13.3	M	33 (3.2)	63.3	2.5	−	+	−	+	+	−
S141F (c.442C>T)	0*	7.7	F	29 (3.6)								
K150R (c.449A>G)†	0.019	2.8	F	25 (4.2)								
R167H (c.500 G>A)	0.002	11.4	M	38 (3.7)	85.4	2.8						
V209I (c.625 G>A)	0.002	3.4	M	27 (5.1)	18.4	1.7	+ S	−	−	−	−	+
R227C (c.679C>T)	0.011	15.5	F	44 (3.9)			−	−	+	+	+	−
R227C (c.679C>T)	0.011	7.5	M	29 (4.0)			+ S	−	+	+	+	+
G238C (c.712G>T)	‡	8.1	M	31 (3.9)	56.9	4.5	+	+	+	+	+	+
R270Q (c.809G>A)	0.002	9.5	F	37 (4.0)	76.3	5.2						
R270W (c.808C>T)	0.001	4.5	M	25 (4.3)	4.7		+ S	−	+	+	−	+
E299G (c.896A>G)	0.002	16.1	F	40 (3.6)	50.5	2.5	−	−	+	+	−	−
M388V (c.1162A>G)	‡	16.5	M	41 (3.7)	118	9.3						
G516S (c.1546G>A)	0.002	11	M	29 (3.1)			+	−	−	+	+	+
S616P (c.1846T>C)	0.019	7.0	F	26 (3.4)	27.9	1.3					+	
G638R (c.1912 G>A)	‡	4.3	F	31 (5.3)	47.5	3.3	−	−	−	−	+	−

MAF (%) in non-Finnish European (NFE) Genome Aggregation Database (gnomAD) exomes (51); 0, variant was detected in gnomAD exomes with MAF = 0 in the NFE sample; *, variant not present in NFE samples but present in samples from other ethnic groups; †, variant not found in any gnomAD exomes; ‡, homozygous variant in a proband from a consanguineous family. F, female, M, male. BMI is weight in kg/height in m² with age- and sex-adjusted BMI SD score shown in parentheses. When fasting plasma glucose and insulin were available, HOMA-IR was calculated. Scores in young obese children are difficult to interpret given the paucity of control data. However, in adults, HOMA-IR >1.9 indicates insulin resistance. Behavioral data were gathered from medical history. + indicates presence of a phenotype. − indicates absence of a phenotype. S indicates speech and language delay. Blank cells indicate insufficient information to record a phenotype.
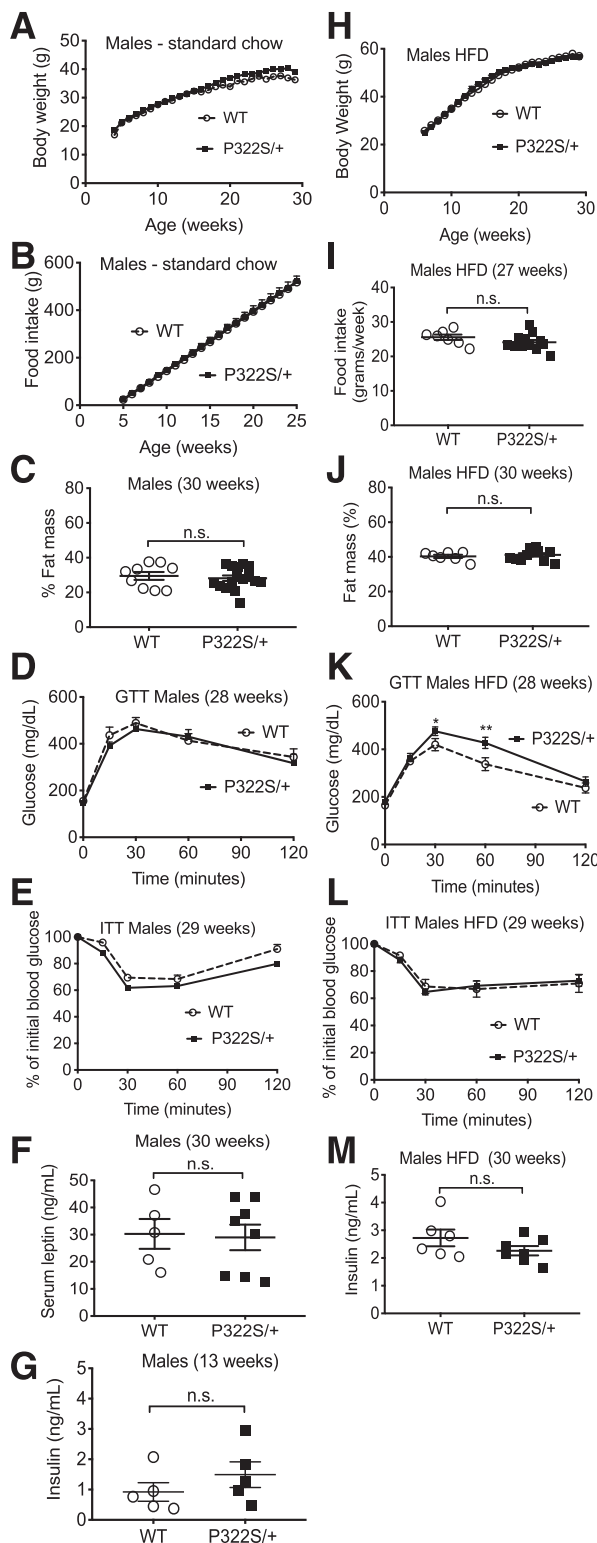
Figure 2—The P322S mutation in SH2B1 leads to impaired glucose homeostasis in male mice challenged with an HFD. *A–G*: Male mice fed standard chow. *A*: Body weight was assessed at weeks 4–29 (*n* = 8 WT, 16 P322S/+). *B*: Food intake was assessed at weeks 5–25 and cumulative food intake graphed (*n* = 7 WT, 8 P322S/+). *C*: Body fat mass was determined at week 30. Percent fat mass was determined by dividing fat mass by body weight (*n* = 9 WT, 16 P322S/+). *D*: GTT was assessed in 28-week-old mice. After a 4-h fast, mice were injected intraperitoneally with D-glucose (2 mg/kg of body weight). Blood glucose was monitored at indicated times

Developmental Lethality in Mice Homozygous for the SH2B1 P322S Mutation

To gain insight into the role of the PH domain of SH2B1 in energy balance and glucose metabolism, we studied the effect of the P322S human obesity-associated SH2B1 PH domain variant in mice. We chose the P322S variant because of its strong association with obesity in the proband family (1), the conservation of P322 across mammals and with the SH2B1 family member SH2B2/APS, its predicted disruptive effect on PH domain function by Provean (RRID:SCR_002182) and PolyPhen (RRID:SCR_013189) analysis, and P322S-dependent deficiencies in SH2B1 function observed in cultured cells (1). We used CRISPR/Cas9-based genome editing to introduce the P322S variant into *Sh2b1* in C57BL/6J mice (Fig. 1*C*). DNA sequencing confirmed germline transmission of the P322S edit (Supplementary Fig. 1*A*). The P322S mutation neither affects the mRNA levels for any of the *Sh2b1* isoforms in the examined tissues (brain, liver, and heart) (Supplementary Fig. 1*B* and *C*) nor alters SH2B1 protein levels or isoform selection in brain tissue (Fig. 1*D* and Supplementary Fig. 1*D*). However, we found that homozygous (P322S/P322S) mice are born at much less than the expected Mendelian ratio (Fig. 1*E*), suggesting that the P322S mutation disrupts SH2B1 PH domain function in a manner that interferes with embryo implantation and/or development. Consistent with this, preliminary data from timed pregnancies reveal that at embryonic day 17, the homozygous embryos (P322S/P322S) are also present at less than the expected Mendelian ratio.

Mice Heterozygous for P322S Exhibit Altered Glucose Tolerance, but Not Altered Energy Balance

In addition to the difficulty of producing sufficient P322S/P322S mice for study, the high rate of embryonic lethality in P322S/P322S mice suggested that the surviving P322S/P322S mice might have underlying poor health, which could interfere with the analysis of their metabolic phenotype. For these reasons, and because human obesity

(*n* = 8 WT, 14 P322S/+). *E*: ITT was assessed in 29-week-old mice. After a 6-h fast, mice were injected intraperitoneally with insulin (1 IU/kg of body weight). Blood glucose was monitored at indicated times (*n* = 8 WT, 15 P322S/+). *F*: At week 30, serum from P322S/+ and WT mice was assayed for leptin (*n* = 5 WT, 8 P322S/+). *G*: Thirteen-week-old mice were fasted overnight (1800–0900 h), and insulin levels were determined (*n* = 5). *H–M*: Male mice fed an HFD. *H*: Starting at week 6, body weight of mice was assessed weekly (*n* = 7 WT, 12 P322S/+). *I*: Food intake in mice was measured during week 27 (*n* = 7 WT, 12 P322S/+). *J*: Body fat mass was determined at week 30 (*n* = 7 WT, 11 P322S/+). *K*: GTT was assessed as in *D* at 28 weeks and blood glucose monitored at the times indicated (*n* = 7 WT, 12 P322S/+). *L*: ITT was assessed as in *C* at 29 weeks and blood glucose monitored at the times indicated (*n* = 6 WT, 10 P322S/+). *M*: At week 30, mice were fasted overnight, and insulin levels were determined (*n* = 6 WT, 7 P322S/+). For all comparisons, data are mean ± SEM. *$*P < 0.05$, **$*P < 0.01$. n.s., not significant.
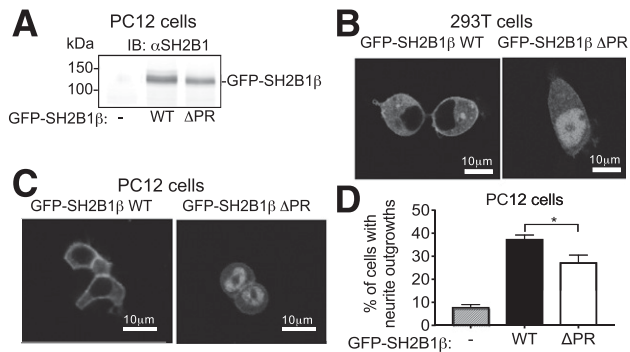
Figure 3—Disruption of the PH domain changes the subcellular localization of SH2B1 and impairs the ability of SH2B1 to enhance NGF-induced neurite outgrowth. *A*: Proteins in whole-cell lysates from PC12 cells transiently expressing the indicated GFP-SH2B1β were immunoblotted with αSH2B1. Migration of molecular weight standards are on the left. IB, immunoblot. *B* and *C*: Live 293T cells and PC12 cells transiently expressing GFP-SH2B1β WT or GFP-SH2B1β ΔPR were imaged by confocal microscopy. *D*: PC12 cells transiently expressing GFP, GFP-SH2B1β WT, or GFP-SH2B1β ΔPR were treated with 25 ng/mL mouse NGF for 2 days, after which neurite outgrowth was assessed. GFP-positive cells were scored for the presence of neurites more than two times the length of the cell body (total of 300 cells/condition/experiment). The percentage of cells with neurites was determined by dividing the number of GFP-positive cells with neurites by the total number of GFP-positive cells counted. Data are mean ± SEM (*n* = 3). *$P < 0.05$.

is linked with heterozygosity for P322S (1), we studied energy balance and glucose homeostasis in heterozygous (P322S/+) male (Fig. 2) and female (Supplementary Fig. 2) mice. We found no difference in food intake, body weight, or adiposity between WT and P322S/+ mice fed standard chow (9% fat) or an HFD (60% fat). However, in contrast to their WT littermates, 28-week-old HFD-fed P322S/+ male and female mice displayed glucose intolerance in an intraperitoneal GTT. Neither insulin concentrations nor the response to an ITT were altered in the P322S/+ animals compared with littermate controls, however. These findings suggest that the PH domain of SH2B1 is important for SH2B1 function, including for the control of glucose homeostasis, but that the resultant metabolic phenotype is less penetrant in the heterozygous state in mice than it is in humans. We thus sought to study mice homozygous for mutations in the SH2B1 PH domain.

Deletion of P317 and R318 in the PH Domain Alters the Subcellular Localization of SH2B1

Because of the early lethality of P322S/P322S mice, we examined the function of another SH2B1 mutation containing a two-amino acid deletion (ΔPR) within the PH domain of SH2B1 (Fig. 1*C* and Supplementary Fig. 1*E*). This mutation arose as a separate line during the generation of the P322S mice.

When transiently expressed as green fluorescent protein (GFP) fusion proteins in PC12 cells, SH2B1β and SH2B1β ΔPR demonstrated similar expression levels (Fig. 3*A*), suggesting that ΔPR does not destabilize the protein.

However, while GFP-SH2B1β localizes primarily to the plasma membrane and cytoplasm in 293T and PC12 cells (as previously shown [22,26]), SH2B1β ΔPR localizes primarily to the nucleus (Fig. 3*B* and *C*). The nuclear localization of SH2B1β ΔPR suggests that the ΔPR mutation alters SH2B1 nuclear cycling to favor retention in the nucleus. We predicted that this altered localization would change the cellular function of SH2B1β ΔPR. Indeed, SH2B1β-dependent NGF-stimulated neurite outgrowth in PC12 cells was decreased in cells expressing SH2B1β ΔPR (Fig. 3*D*). Thus, disruption of the PH domain by the ΔPR mutation alters the subcellular distribution of SH2B1β and impairs the ability of SH2B1β to enhance neurotrophic factor–induced neurite outgrowth.

Obesity, Hyperphagia, and Disrupted Glucose Homeostasis in Mice Homozygous for the SH2B1 ΔPR Mutation

We examined the phenotype of the mice containing the ΔPR mutation with the hope that this mutation might produce a less dramatic reproductive phenotype than that observed with P322S in the homozygous state, allowing us to examine the effects of the ΔPR mutation on energy balance and glucose homeostasis in homozygous mice. As with the P322S mutation, ΔPR did not affect the mRNA levels for any of the *Sh2b1* isoforms in the tissues tested (brain or heart) (Fig. 4*A*). At the protein level, the ΔPR mutation did not alter the relative levels of the different isoforms in brain tissue, although levels of SH2B1 protein were somewhat reduced (Fig. 4*B*). Importantly, in contrast to P322S/P322S mice, ΔPR/ΔPR homozygous mice were born and survived at the expected Mendelian frequency (Supplementary Fig. 1*F*), permitting us to examine the effect of this SH2B1 PH domain mutation in the homozygous state.

ΔPR/ΔPR mice fed standard chow exhibit significantly increased body weight compared with their WT littermates (Fig. 4*C* and *D*). By 20 weeks of age (Fig. 4*C*), ΔPR/ΔPR male mice were 15 g (>40%) heavier than their WT littermates, while female ΔPR/ΔPR mice were ~9 g (~35%) heavier than their WT littermates. It should be noted that we do not believe that the reduced levels of SH2B1 protein in the ΔPR/ΔPR mice can account for the increased obesity detected in ΔPR/ΔPR mice because heterozygote *Sh2b1*$^{-/+}$ mice are not obese (5). Body length was not significantly different in preliminary studies (Supplementary Fig. 1*G* and *H*). Overall adiposity (Fig. 4*E* and *F*) as well as circulating leptin concentrations (Fig. 4*G*) were increased in ΔPR/ΔPR homozygotes but not lean body mass (Fig. 4*H*). The heterozygous (ΔPR/+) male and female mice showed no significant increase in adiposity (Fig. 4*F*). However, ΔPR/+ males had a slight increase in circulating leptin levels (Fig. 4*G*), suggesting that in males, even a single copy of the ΔPR mutation may be sufficient to produce a minor effect on energy balance.

Increased food intake (assessed at 18–20 weeks) is observed in ΔPR/ΔPR male and female mice compared with their WT and ΔPR/+ littermates (Fig. 5*A*), while VO$_2$
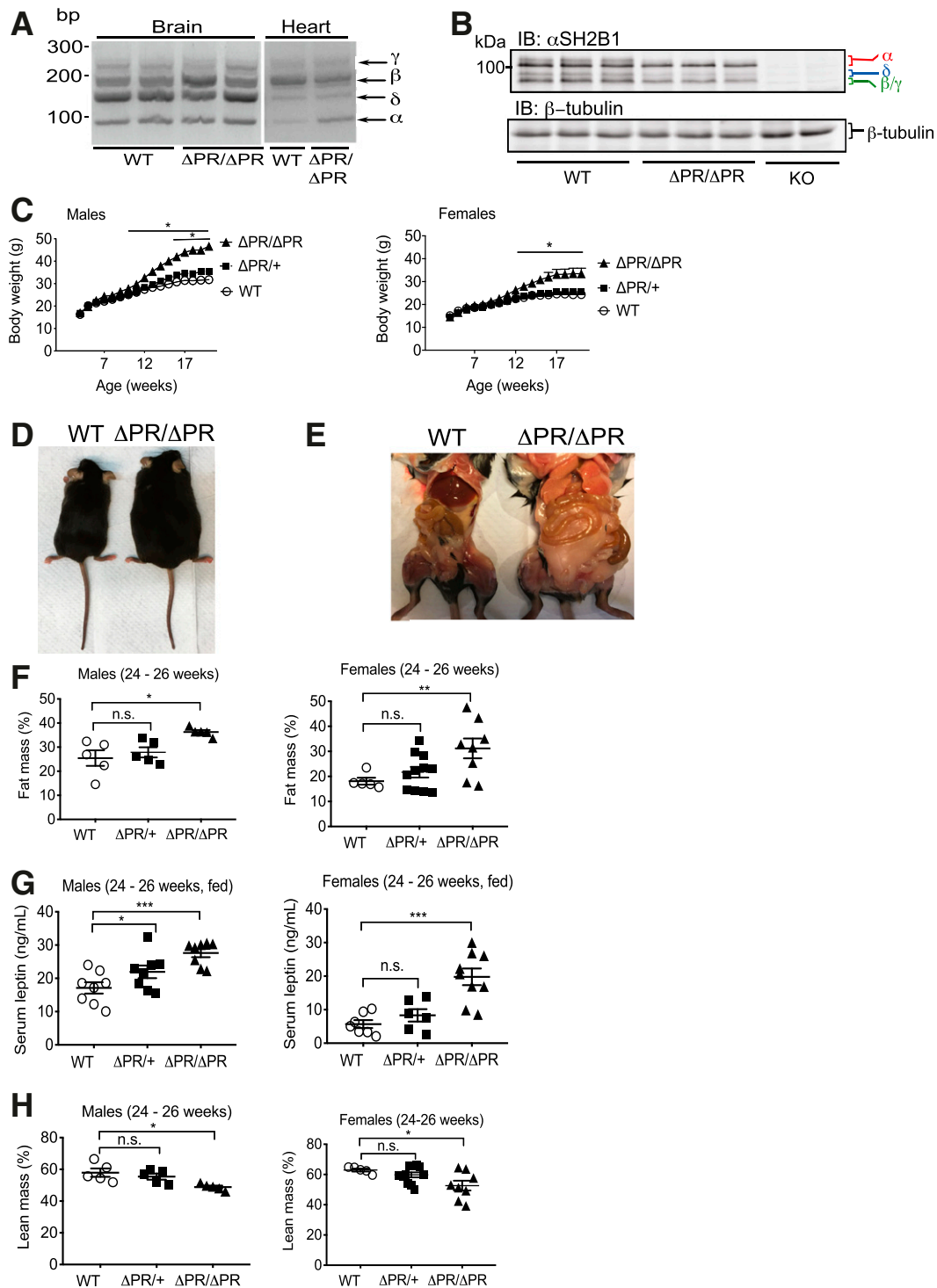
Figure 4—Disruption of the PH domain in SH2B1 results in obesity. *A*: mRNA was extracted from brain and heart tissue of WT and ΔPR/ΔPR male mice. The migration of DNA standards (left) and isoform-specific PCR products (right) are shown. bp, base pair. *B*: Proteins in brain lysates from *Sh2b1* WT, ΔPR/ΔPR, and KO male mice were immunoblotted with αSH2B1 and αβ-tubulin. The migration of the 100-kDa protein standard (left) and the four known isoforms of SH2B1 and β-tubulin (right) are shown. IB, immunoblot. *C*: Body weight was assessed weekly starting at week 4 (males: *n* = 9 WT, 14 ΔPR/+, 9 ΔPR/ΔPR; females: *n* = 7 WT, 16 ΔPR/+, 11 ΔPR/ΔPR). *D*: Representative *Sh2b1* WT and ΔPR/ΔPR male mice (6 months). *E*: Perigonadal fat of representative *Sh2b1* WT and ΔPR/ΔPR male littermates (6 months). *F* and *H*: Body fat and lean mass was determined at weeks 24–26. Percent fat or lean mass was determined by dividing by body weight (males: *n* = 5 WT, ΔPR/+, and ΔPR/ΔPR; females: *n* = 5 WT, 11 ΔPR/+, 8 ΔPR/ΔPR). *G*: At weeks 24–26, serum from *Sh2b1* WT, ΔPR/+, and ΔPR/ΔPR male and female mice was assayed for leptin (males: *n* = 8 WT, ΔPR/+, and ΔPR/ΔPR; females: *n* = 7 WT, 6 ΔPR/+, 9 ΔPR/ΔPR). For all comparisons, data are mean ± SEM. *$P < 0.05$, **$P < 0.01$, ***$P < 0.001$. n.s., not significant.
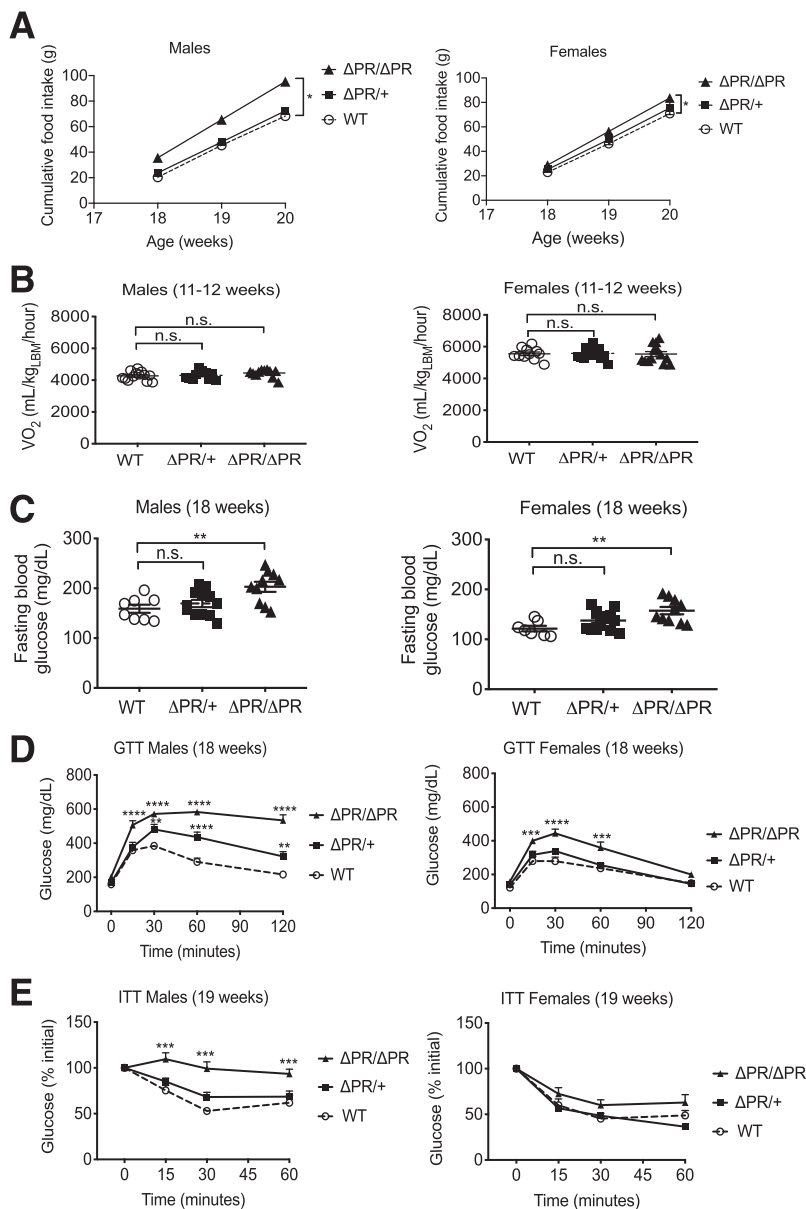
Figure 5—The ΔPR mice exhibit increased food intake and reduced glucose tolerance and insulin sensitivity. *A*: Food intake was measured for weeks 18–20 and cumulative food intake graphed (males: *n* = 11 WT, 10 ΔPR/+, 7 ΔPR/ΔPR; females: *n* = 6 WT, 9 ΔPR/+, and ΔPR/ΔPR). Same cohort of mice as in Fig. 4. *B*: Energy expenditure was assessed at 11–12 weeks using a Comprehensive Lab Animal Monitoring System. VO_2 was normalized to lean body mass (LBM) (males: *n* = 13 WT, 10 ΔPR/+, 11 ΔPR/ΔPR; females: *n* = 11 WT, 15 ΔPR/+, 13 ΔPR/ΔPR). *C*: At week 18, mice were fasted for 4 h, and blood glucose was measured (males: *n* = 8 WT, 12 ΔPR/+, 10 ΔPR/ΔPR; females: *n* = 7 WT, 14 ΔPR/+, 10 ΔPR/ΔPR). *D*: GTT was assessed at 18 weeks as in Fig. 2*D* and blood glucose monitored at times indicated (males: *n* = 8 WT, 12 ΔPR/+, 10 ΔPR/ΔPR; females: *n* = 7 WT, 14 ΔPR/+, 10 ΔPR/ΔPR). *E*: ITT was assessed at 19 weeks as in Fig. 2*E* and blood glucose monitored at the times indicated (males: *n* = 9 WT, 14 ΔPR/+, 11 ΔPR/ΔPR; females: *n* = 6 WT, 13 ΔPR/+, 11 ΔPR/ΔPR). Same cohort of mice as Fig. 4. For all comparisons, data are mean ± SEM. *$P < 0.05$, **$P < 0.01$, ***$P < 0.001$, ****$P < 0.0001$ compared with WT littermates. n.s., not significant.

(at 11–12 weeks of age) (Fig. 5*B*), respiratory exchange ratio (data not shown), and locomotor activity (data not shown) were not altered. On the basis of these data and the previous finding that *Sh2b1* KO mice are obese primarily as a consequence of increased food intake (5), we believe it most likely that the ΔPR mutation caused obesity in the mice primarily as a consequence of increasing food intake rather than decreasing energy expenditure.

Glucose Tolerance and Insulin Resistance of ΔPR/ΔPR Mice

We initially examined parameters of glycemic control in ΔPR mice at 18–19 weeks of age. In homozygous ΔPR/ΔPR mice, hyperglycemia at baseline was evident (Fig. 5*C*) as well as impaired glucose tolerance (male and female mice) and insulin resistance (male mice) in intraperitoneal GTT and ITT, respectively (Fig. 5*D* and *E*). Male heterozygous ΔPR/+ mice (like P322S/+ mice) also displayed impaired
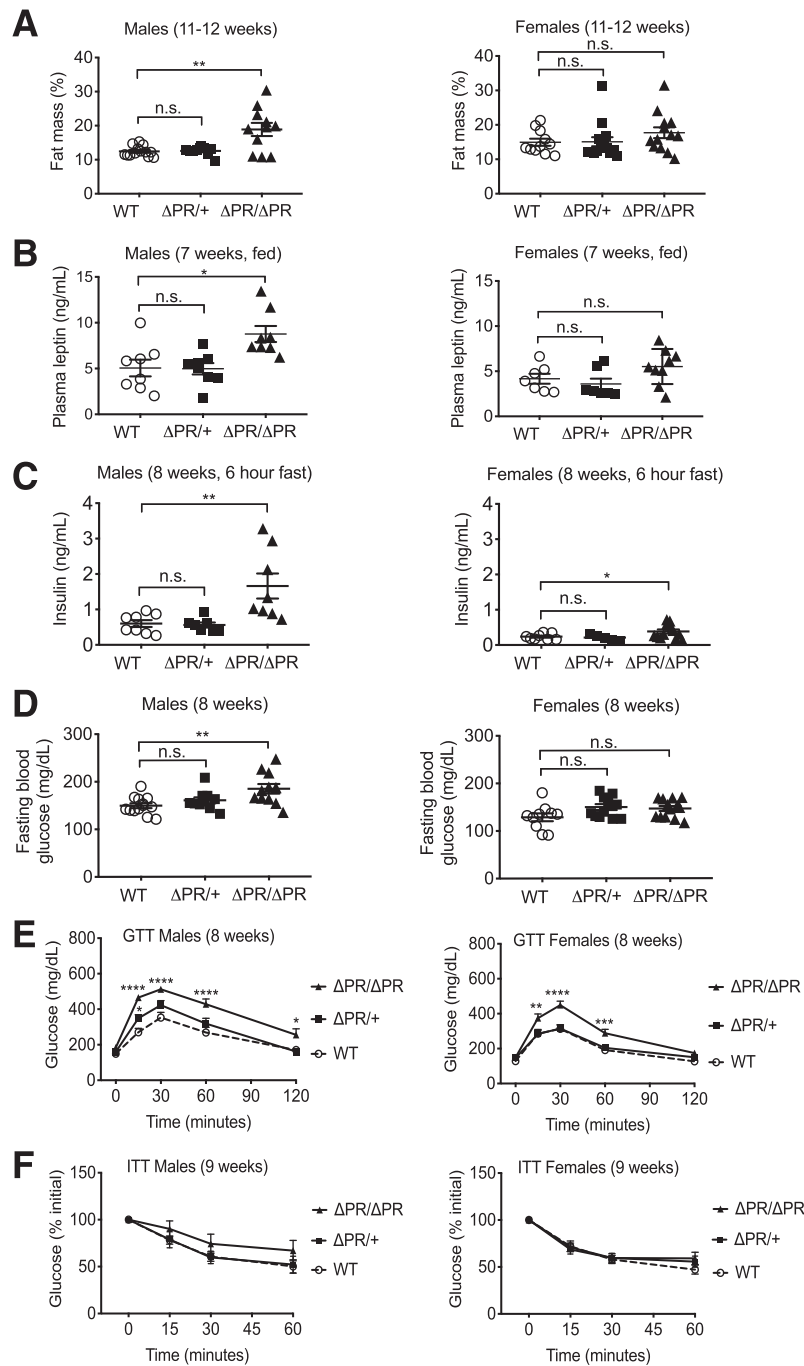
Figure 6—ΔPR female mice exhibit reduced glucose tolerance before the onset of obesity. A: Body fat mass was determined at weeks 11–12. Percent fat mass was determined by dividing the mass by body weight (males: n = 13 WT, 10 ΔPR/+, 11 ΔPR/ΔPR; females: n = 11 WT, 15 ΔPR/+, 13 ΔPR/ΔPR). B: At week 7, serum from WT, ΔPR/+, and ΔPR/ΔPR male mice was assayed for leptin (males: n = 8 WT and ΔPR/ΔPR, 7 ΔPR/+; females: n = 8 WT, 5 ΔPR/+, 12 ΔPR/ΔPR). C: Eight-week-old mice were fasted for 6 h, and insulin levels were determined (males: n = 11 WT, 9 ΔPR/+, 10 ΔPR/ΔPR; females: n = 9 WT, 11 ΔPR/+, 13 ΔPR/ΔPR). D: At week 8, mice were fasted for 4 h, and blood glucose was measured (males: n = 13 WT, 10 ΔPR/+, 11 ΔPR/ΔPR; females: n = 10 WT, 13 ΔPR/+, 12 ΔPR/ΔPR). E: In a separate study, GTT was assessed at 8 weeks as in Fig. 2D and blood glucose monitored at the times indicated (males: n = 13 WT, 10 ΔPR/+, 11 ΔPR/ΔPR; females: n = 10 WT, 13 ΔPR/+, 12 ΔPR/ΔPR). F: ITT was assessed at 9 weeks as in Fig. 2E and blood glucose monitored at the times indicated (males: n = 11 WT, 9 ΔPR/+, 10 ΔPR/ΔPR; females: n = 9 WT, 11 ΔPR/+, 13 ΔPR/ΔPR). Same cohort of mice as Fig. 5B. For all comparisons, data are mean ± SEM. *$P < 0.05$, **$P < 0.01$, ***$P < 0.001$, ****$P < 0.0001$ compared with WT littermates. n.s., not significant.

glucose tolerance (Fig. 5D), although other parameters of glucose homeostasis were not different from WT littermates.

Because the disruption of glucose homeostasis in the aged ΔPR/ΔPR mice presumably resulted (at least in part) from their increased adiposity, we examined glucose

homeostasis in young preobese mice to define any adiposity-independent effects of SH2B1 ΔPR on glucose homeostasis. We examined the adiposity of younger ΔPR/ΔPR mice to determine an age at which we might examine glucose homeostasis without it being confounded by increased adiposity. At 11–12 weeks of age, adiposity was already increased in male ΔPR/ΔPR mice but not detectably increased in female ΔPR/ΔPR mice (Fig. 6A). By 7 weeks, leptin levels were increased in male, but not female, ΔPR/ΔPR mice (Fig. 6B). We thus examined glucose homeostasis in ΔPR/ΔPR mice at 8 weeks of age, revealing hyperinsulinemia and glucose intolerance (with unchanged insulin tolerance) in both male and female ΔPR/ΔPR mice (Fig. 6C–F). The hyperinsulinemia and glucose intolerance in the presence of unchanged leptin and adiposity in young preobese females suggest that the ΔPR mutation interferes with glucose homeostasis independently of adiposity. Taken together, our results suggest that in obese ΔPR mice, the ΔPR mutation likely interferes with glucose homeostasis both independently of adiposity and secondary to the effects of adiposity on energy balance.

DISCUSSION

The identification of four human obesity-associated variants in the PH domain-encoding region of *SH2B1*, the fact that the three individuals with PH domain variants whose behavior has been documented all displayed behavioral abnormalities (1,2, and the present study), and the fact that the three individuals with variants in or near the PH domain had HOMA-IR scores suggesting severe insulin resistance and

risk of type 2 diabetes, highlight the importance of the PH domain in SH2B1 function. The lethality of the human obesity-associated P322S mutation in the PH domain of SH2B1 in homozygous P322S/P322S mice demonstrates the importance of this mutation for SH2B1 function in vivo. Similarly, the obesity and diabetes observed in ΔPR/ΔPR mice highlight the importance of the SH2B1 PH domain for SH2B1-mediated metabolic control. The adiposity-independent glucose intolerance of young ΔPR/ΔPR female mice before the onset of obesity as well as of P322S/+ and ΔPR/+ mice also reveals the importance of SH2B1 and its PH domain for the control of glucose homeostasis independent of body weight, as previously suggested from the phenotype of humans bearing mutations in SH2B1 (1,2).

On the basis of the increased food intake of ΔPR/ΔPR mice and the findings in the *Sh2b1* KO mice (5), we believe it likely that the increased body weight of the ΔPR/ΔPR mice is due to impaired function of SH2B1 in the hypothalamus. However, SH2B1 is also expressed in the periphery. The increased insulin concentrations with glucose intolerance in young, nonobese female ΔPR/ΔPR mice suggest alterations in tissues that control glucose uptake. However, the presence of glucose intolerance despite the increased insulin levels is consistent with the islets of ΔPR/ΔPR mice having an impaired ability to fully compensate for those alterations (41,42).

While humans heterozygous for P322S exhibit severe obesity, P322S/+ mice display mild glucose intolerance only in aged, HFD-fed animals. Because the region surrounding P322 is conserved between mice and humans
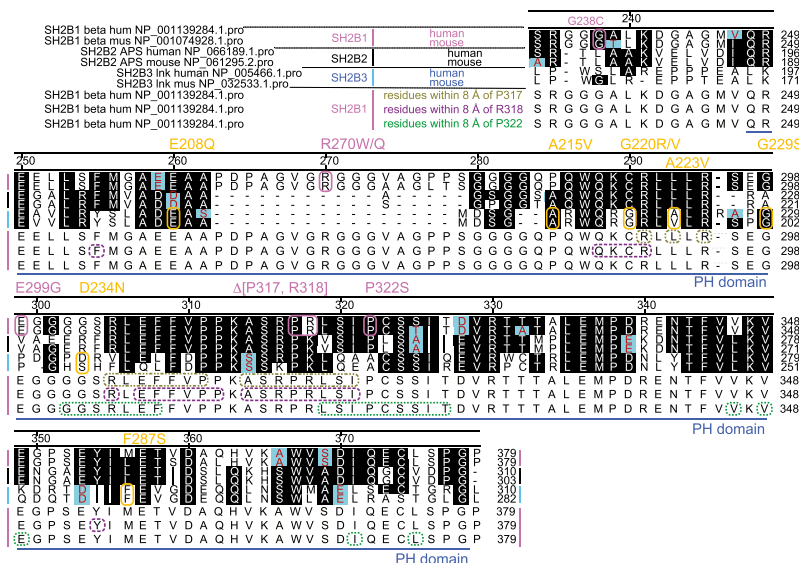

Figure 7—ClustalW analysis and modeling of the three-dimensional structure of the PH domain of SH2B1. ClustalW of SH2B1, SH2B2/APS, and SH2B3/Lnk in the region included in the NMR structure of SH2B2/APS. Homologous residues are highlighted in black, and functionally homologous residues are cyan. The PH domain is indicated by the blue line below the sequences. P317, R318 in SH2B1 and the residues in SH2B1 for which variants are associated with obesity are indicated by magenta ovals. The variants are noted above the ClustalW. Residues within 8 Å of P317 in SH2B1 (P240 in SH2B3/Lnk) are denoted by taupe ovals. Residues within 8 Å of R318 in SH2B1 (K241 in SH2B3/Lnk) in the 3-dimensional structure (Video 1) are denoted by purple ovals. Residues within 8 Å of P322 in SH2B1 (P245 in SH2B3/Lnk) are denoted by green ovals. hum, human; mus, mouse.

(Fig. 7), it is unlikely that the more modest phenotype of P322S/+ mice compared with humans reflects species differences that result in structural changes in the SH2B1 PH domain, per se, but rather that PH domain binding partners may have different tolerances for P322S in mice and humans and/or that human physiology adapts more poorly to the resultant alterations in SH2B1 function. Consistent with the importance of the PH domain for the function of SH2B family members, at least nine point mutations (E208Q/E, A215V, G220V/R, A223V, G229S, D234N, F287S) have been identified in the PH domain of the SH2B1 ortholog SH2B3/Lnk in patients with myeloproliferative neoplasms (43–48) (Fig. 7).

To gain insight into how the SH2B1 P322S mutation or deletion of residues P317 and R318 in SH2B1 might regulate the function of the PH domain in SH2B1, we performed ClustalW analysis of SH2B family members and analyzed a model of SH2B1 that was based on the NMR structure of the PH domain of the SH2B1 family member SH2B2/APS (49). ClustalW analysis of the PH domains of the SH2B family members reveals that the PH domains are highly conserved (Fig. 7). In the model, residues P317, R318, and P322S in SH2B1 are on an exterior surface of the PH domain (Video 1). This surface is presumably a binding interface that interacts with either another region in SH2B1 or another protein. Another human obesity-associated variant in SH2B1 (E299G) as well as five of the human myeloproliferative neoplasm-associated variants in SH2B3/Lnk (G220V/R, A223V, G229S, and D234N) are in proximity to P317, R318, and P322 in SH2B1. In addition, eight of the human variants (E208Q, A215V, G220 V/R, G229S, D234N in SH2B3/Lnk and E299G, P322S in SH2B1) as well as P317 and R318 in SH2B1 are on or in proximity to this putative protein-binding interface (Fig. 7 and Video 1).

The number of human variants in SH2B1 and SH2B3 in this region of the PH domain suggests that small structural changes in this region as a result of mutation or other modification have the potential to produce substantial functional consequences. Because the residues corresponding to P317 and R318 in SH2B1 are on the surface of the PH domain and do not substantially change the direction of the loop, the P317, R318 deletion in SH2B1 would shorten the loop but not severely damage the overall structure. However, the deletion would be expected to diminish stabilization of the turn provided by the predicted π-π stacking between residues P317 and F309 in SH2B1. In addition, the deletion would be expected to alter the shape and electrostatics of the interface surface in the region of P317 and R318 in SH2B1.

Because SH2B1 from humans and mice share 95% sequence identity, with only one conservative difference (S325T) near P322 (Fig. 7), the structures in mouse and human are expected to be nearly identical. Therefore, the
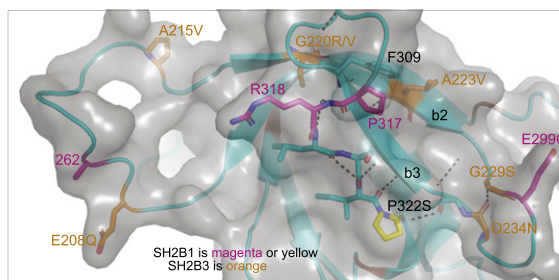
Video 1—This image is from a video available online at https://bcove .video/2lNxwhM. Modeling of the three-dimensional structure of the PH domain of SH2B1. A model of human SH2B1 was created by overlaying the sequence of the PH domain of human SH2B1 onto the mouse structure of APS. The two PH domain sequences are 75% similar (55.3% identical). The SH2B1 model is missing a single amino acid insertion at residue 296 and the 16-residue insertion at residue 262 which contains the R270W/Q human variant in SH2B1. The amino acid sequence of residues surrounding the P322 site is highly conserved between the two proteins. P322 is shown as yellow sticks. The other human variants in SH2B1 as well as residues P317 and R318 are magenta sticks. The human variants in Lnk are orange sticks. Differences between mouse and human SH2B1 are brown (no sticks). Oxygen atoms are red and nitrogen blue. β-Pleated sheets, α-helices, connecting loops, and hydrogen bonds in the region between the N-terminal end of β-strand 2 and the loop containing P317, R318, and P322 are indicated. The surface of the PH domain is tinted gray. P322 in SH2B1 is within 8 Å of the site of the D234N variant in SH2B3/Lnk. The turn that contains D234N also contains the G229S variant in SH2B3/Lnk and the E299G variant in SH2B1. P317 and R318 in SH2B1 are within 8 Å of the site of G220 R/V and A223V in SH2B3/Lnk. This region is stabilized by π-π stacking between P317 and F309 in SH2B1 (P248 and F240 in Lnk) and a network of hydrogen bonds.

more modest phenotypes of P322S/+ mice compared with humans may be due to differences in the affinity of PH domain binding partners. The mouse binding partners may be able to accommodate the P322S mutation better than human binding partners, and/or human physiology adapts more poorly to the resultant alterations in SH2B1 function. Given the different phenotypes produced by the P322S and ΔPR mutations in mice, we postulate that the two mutations alter the structure of the SH2B1 PH domain in different ways to produce distinct changes in cell physiology. That relatively small changes in the PH domain, predicted to have only minor effects on PH domain structure, cause a rather profound effect on SH2B1β localization at the cellular level and energy balance and glucose homeostasis at the whole-animal level provides some of the first real evidence of the importance of the PH domain in SH2B1 function. While SH2B1β has been shown to cycle through the nucleus, it is generally found at the plasma membrane and in the cytoplasm (22,23,26). The accumulation of SH2B1β ΔPR in the nucleus indicates that the ΔPR deletion greatly alters the ratio between nuclear import and nuclear export of SH2B1β. Consistently, the ΔPR mutation as well as many of the other human obesity-associated SH2B1 variants impair the ability of SH2B1β to promote neurotrophic factor–induced neurite outgrowth of PC12 cells. Because neurite outgrowth in PC12 cells shares many properties

with the formation of axons and/or dendrites (50), and because the *Sh2b1* KO mice have impaired leptin signaling, it will be important in the future to examine the impact of SH2B1 PH domain changes on the structure of neurons that control energy balance.

Duality of Interest. No potential conflicts of interest relevant to this article were reported.

Author Contributions. A.F. directed and conducted experiments, analyzed data, and prepared the manuscript. A.F. and L.S.A. designed and generated the mice. A.F., L.S.A., I.S.F, M.G.M., and C.C.-S. developed the concept, designed experiments, and interpreted the data. L.S.A. and J.S. analyzed the model of the PH domain (Fig. 7 and Video 1). L.S.A., I.S.F., M.G.M., and C.C.-S. made revisions to the manuscript. L.K.J.S. and E.M.d.O. characterized the human mutations in cells (Fig. 1*B*). A.E.M. helped to regenotype the mice. A.E.M., L.C.D., G.C., and Y.H. helped to measure body weight and food intake (Figs. 2*A*, *B*, *H*, and *I*, 4*C*, and 5*A* and Supplementary Fig. 2*A*, *B*, *F*, and *G*). P.B.V. conducted neurite outgrowth experiments (Fig. 3*D*) and helped with experiments for Fig. 3*A* and *C*. R. M.J. conducted preliminary experiments for Fig. 3*B*. J.M.C. made the GFP-SH2B1β WT and GFP-SH2B1β ΔPR constructs (Fig. 3). J.M.K., E.H., and I.S.F. performed the clinical studies in mutation carriers (Fig. 1*A* and Table 1). I.B. and I.S.F. performed the genetic studies (Fig. 1*A* and Table 1). E.S.C. maintained mouse colonies and helped to genotype mice and collect blood samples (Figs. 4*G* and 6*B*). All authors approved the final content. I.S.F. and C.C.-S. are the guarantors of this work and, as such, had full access to all the data in the study and take responsibility for the integrity of the data and the accuracy of the data analysis.

Prior Presentation. Parts of this work were presented in poster form or as short oral presentations at the 2015 Neurotrophic Factors Gordon Research Conference, Newport, RI, 31 May–5 June 2015; 2016 Keystone Symposium on Molecular and Cellular Biology—Axons: From Cell Biology to Pathology, Santa Fe, NM, 24–27 January 2016; 2017 Keystone Symposium on Molecular and Cellular Biology: Neuronal Control of Appetite, Metabolism and Weight, Copenhagen, Denmark, 9–13 May 2017; 2017 Society for Advancement of Chicanos/Hispanics and Native Americans in Science (SACNAS) National Diversity in STEM Conference, Salt Lake City, UT, 19–21 October 2017; 2018 Molecular and Cellular Neurobiology Gordon Research Conference, Hong Kong, China, 1–6 July 2018; 2018 SACNAS National Diversity in STEM Conference, San Antonio, TX, 11–13 October 2018; Experimental Biology 2018, San Diego, CA, 21–25 April 2018; and 2019 Keystone Symposium on Molecular and Cellular Biology: Functional Neurocircuitry of Feeding Disorders, Banff, AB, Canada, 10–14 February 2019.

References

1. Doche ME, Bochukova EG, Su HW, et al. Human SH2B1 mutations are associated with maladaptive behaviors and obesity [published correction appears in J Clin Invest 2013;123:526]. J Clin Invest 2012;122:4732–4736

2. Pearce LR, Joe R, Doche ME, et al. Functional characterization of obesity-associated variants involving the α and β isoforms of human SH2B1. Endocrinology 2014;155:3219–3226

3. Duan C, Yang H, White MF, Rui L. Disruption of the SH2-B gene causes age-dependent insulin resistance and glucose intolerance. Mol Cell Biol 2004;24: 7435–7443

4. Jiang L, Su H, Keogh JM, et al. Neural deletion of Sh2b1 results in brain growth retardation and reactive aggression. FASEB J 2018;32:1830–1840

5. Ren D, Li M, Duan C, Rui L. Identification of SH2-B as a key regulator of leptin sensitivity, energy balance, and body weight in mice. Cell Metab 2005;2:95–104

6. Ren D, Zhou Y, Morris D, Li M, Li Z, Rui L. Neuronal SH2B1 is essential for controlling energy and glucose homeostasis. J Clin Invest 2007;117: 397–406

7. Kurzer JH, Argetsinger LS, Zhou Y-J, Kouadio J-L, O'Shea JJ, Carter-Su C. Tyrosine 813 is a site of JAK2 autophosphorylation critical for activation of JAK2 by SH2-B β. Mol Cell Biol 2004;24:4557–4570

8. Li Z, Zhou Y, Carter-Su C, Myers MG Jr., Rui L. SH2B1 enhances leptin signaling by both Janus kinase 2 Tyr^{813} phosphorylation-dependent and -independent mechanisms. Mol Endocrinol 2007;21:2270–2281

9. Nelms K, O'Neill TJ, Li S, Hubbard SR, Gustafson TA, Paul WE. Alternative splicing, gene localization, and binding of SH2-B to the insulin receptor kinase domain. Mamm Genome 1999;10:1160–1167

10. Qian X, Riccio A, Zhang Y, Ginty DD. Identification and characterization of novel substrates of Trk receptors in developing neurons. Neuron 1998;21:1017–1029

11. Riedel H, Wang J, Hansen H, Yousaf N. PSM, an insulin-dependent, pro-rich, PH, SH2 domain containing partner of the insulin receptor. J Biochem 1997;122: 1105–1113

12. Rui L, Carter-Su C. Identification of SH2-bbeta as a potent cytoplasmic activator of the tyrosine kinase Janus kinase 2. Proc Natl Acad Sci U S A 1999;96: 7172–7177

13. Shih CH, Chen CJ, Chen L. New function of the adaptor protein SH2B1 in brain-derived neurotrophic factor-induced neurite outgrowth. PLoS One 2013;8: e79619

14. Qian X, Ginty DD. SH2-B and APS are multimeric adapters that augment TrkA signaling. Mol Cell Biol 2001;21:1613–1620

15. Kurzer JH, Saharinen P, Silvennoinen O, Carter-Su C. Binding of SH2-B family members within a potential negative regulatory region maintains JAK2 in an active state. Mol Cell Biol 2006;26:6381–6394

16. Duan C, Li M, Rui L. SH2-B promotes insulin receptor substrate 1 (IRS1)- and IRS2-mediated activation of the phosphatidylinositol 3-kinase pathway in response to leptin. J Biol Chem 2004;279:43684–43691

17. Morris DL, Cho KW, Zhou Y, Rui L. SH2B1 enhances insulin sensitivity by both stimulating the insulin receptor and inhibiting tyrosine dephosphorylation of insulin receptor substrate proteins. Diabetes 2009;58:2039–2047

18. Diakonova M, Gunter DR, Herrington J, Carter-Su C. SH2-Bbeta is a Rac-binding protein that regulates cell motility. J Biol Chem 2002;277:10669–10677

19. Joe RM, Flores A, Doche ME, et al. Phosphorylation of the unique C-terminal tail of the alpha isoform of the scaffold protein SH2B1 controls the ability of SH2B1α to enhance nerve growth factor function. Mol Cell Biol 2018;38:e00277-17

20. Timper K, Brüning JC. Hypothalamic circuits regulating appetite and energy homeostasis: pathways to obesity. Dis Model Mech 2017;10:679–689

21. Rui L, Herrington J, Carter-Su C. SH2-B is required for nerve growth factor-induced neuronal differentiation. J Biol Chem 1999;274:10590–10594

22. Chen L, Carter-Su C. Adapter protein SH2-B β undergoes nucleocytoplasmic shuttling: implications for nerve growth factor induction of neuronal differentiation. Mol Cell Biol 2004;24:3633–3647

23. Maures TJ, Chen L, Carter-Su C. Nucleocytoplasmic shuttling of the adapter protein SH2B1β (SH2-Bbeta) is required for nerve growth factor (NGF)-dependent neurite outgrowth and enhancement of expression of a subset of NGF-responsive genes. Mol Endocrinol 2009;23:1077–1091

24. Yousaf N, Deng Y, Kang Y, Riedel H. Four PSM/SH2-B alternative splice variants and their differential roles in mitogenesis. J Biol Chem 2001;276:40940–40948

25. Maures TJ. *Molecular mechanisms by which adapter protein SH2B1β facilitates NGF-dependent neuronal differentiation*. Ann Arbor, MI, Cellular and Molecular Biology, University of Michigan, 2008, p. 261

26. Maures TJ, Su H-W, Argetsinger LS, Grinstein S, Carter-Su C. Phosphorylation controls a dual-function polybasic nuclear localization sequence in the adapter protein SH2B1β to regulate its cellular function and distribution. J Cell Sci 2011;124:1542–1552

27. Baumeister MA, Rossman KL, Sondek J, Lemmon MA. The Dbs PH domain contributes independently to membrane targeting and regulation of guanine nucleotide-exchange activity. Biochem J 2006;400:563–572

28. Klein DE, Lee A, Frank DW, Marks MS, Lemmon MA. The Pleckstrin homology domains of dynamin isoforms require oligomerization for high affinity phosphoinositide binding. J Biol Chem 1998;273:27725–27733

29. Lemmon MA. Phosphoinositide recognition domains. Traffic 2003;4:201–213

30. Park WS, Heo WD, Whalen JH, et al. Comprehensive identification of PIP3-regulated PH domains from C. elegans to H. sapiens by model prediction and live imaging. Mol Cell 2008;30:381–392

31. Farooqi IS, Keogh JM, Yeo GS, Lank EJ, Cheetham T, O'Rahilly S. Clinical spectrum of obesity and mutations in the melanocortin 4 receptor gene. N Engl J Med 2003;348:1085–1095

32. Wheeler E, Huang N, Bochukova EG, et al. Genome-wide SNP and CNV analysis identifies common and low-frequency variants associated with severe early-onset obesity. Nat Genet 2013;45:513–517

33. Hendricks AE, Bochukova EG, Marenne G, et al.; Understanding Society Scientific Group; EPIC-CVD Consortium; UK10K Consortium. Rare variant analysis of human and rodent obesity genes in individuals with severe childhood obesity. Sci Rep 2017;7:4394

34. Matthews DR, Hosker JP, Rudenski AS, Naylor BA, Treacher DF, Turner RC. Homeostasis model assessment: insulin resistance and beta-cell function from fasting plasma glucose and insulin concentrations in man. Diabetologia 1985;28:412–419

35. Muniyappa R, Lee S, Chen H, Quon MJ. Current approaches for assessing insulin sensitivity and resistance in vivo: advantages, limitations, and appropriate usage. Am J Physiol Endocrinol Metab 2008;294:E15–E26

36. Ran FA, Hsu PD, Wright J, Agarwala V, Scott DA, Zhang F. Genome engineering using the CRISPR-Cas9 system. Nat Protoc 2013;8:2281–2308

37. Truett GE, Heeger P, Mynatt RL, Truett AA, Walker JA, Warman ML. Preparation of PCR-quality mouse genomic DNA with hot sodium hydroxide and tris (HotSHOT). Biotechniques 2000;29:52, 54

38. Li Q, Cao X, Qiu H-Y, et al. A three-step programmed method for the identification of causative gene mutations of maturity onset diabetes of the young (MODY). Gene 2016;588:141–148

39. Sheng L, Liu Y, Jiang L, et al. Hepatic SH2B1 and SH2B2 regulate liver lipid metabolism and VLDL secretion in mice. PLoS One 2013;8:e83269

40. van der Aa MP, Fazeli Farsani S, Kromwijk LA, de Boer A, Knibbe CA, van der Vorst MM. How to screen obese children at risk for type 2 diabetes mellitus? Clin Pediatr (Phila) 2014;53:337–342

41. Chen Z, Morris DL, Jiang L, Liu Y, Rui L. SH2B1 in β-cells promotes insulin expression and glucose metabolism in mice. Mol Endocrinol 2014;28:696–705

42. Chen Z, Morris DL, Jiang L, Liu Y, Rui L. SH2B1 in β-cells regulates glucose metabolism by promoting β-cell survival and islet expansion. Diabetes 2014;63:585–595

43. Hurtado C, Erquiaga I, Aranaz P, et al. LNK can also be mutated outside PH and SH2 domains in myeloproliferative neoplasms with and without V617FJAK2 mutation. Leuk Res 2011;35:1537–1539

44. Lasho TL, Mudireddy M, Finke CM, et al. Targeted next-generation sequencing in blast phase myeloproliferative neoplasms. Blood Adv 2018;2:370–380

45. McMullin MF, Cario H. LNK mutations and myeloproliferative disorders. Am J Hematol 2016;91:248–251

46. Oh ST, Gotlib J. JAK2 V617F and beyond: role of genetics and aberrant signaling in the pathogenesis of myeloproliferative neoplasms. Expert Rev Hematol 2010;3:323–337

47. Pardanani A, Lasho T, Finke C, Oh ST, Gotlib J, Tefferi A. LNK mutation studies in blast-phase myeloproliferative neoplasms, and in chronic-phase disease with TET2, IDH, JAK2 or MPL mutations. Leukemia 2010;24:1713–1718

48. Tefferi A, Lasho TL, Guglielmelli P, et al. Targeted deep sequencing in polycythemia vera and essential thrombocythemia. Blood Adv 2016;1:21–30

49. Li H, Tochio N, Koshiba S, Inoue M, Kigawa T, Yokoyama S. 2004 Solution structure of the pleckstrin homology domain of mouse APS [Solution NMR structure online]. Available from https://www.ncbi.nlm.nih.gov/Structure/pdb/1V5M. Accessed 9 October 2018

50. Vaudry D, Stork PJ, Lazarovici P, Eiden LE. Signaling pathways for PC12 cell differentiation: making the right connections. Science 2002;296:1648–1649

51. Karczewski KJ, Francioli LC, Tiao G, et al. Variation across 141,456 human exomes and genomes reveals the spectrum of loss-of-function intolerance across human protein-coding genes. bioRxiv 2019:531210